D45

N79-24046

STABLE DIELECTRIC CHARGE DISTRIBUTIONS FROM FIELD ENHANCEMENT OF SECONDARY EMISSION*

James W. Robinson
The Pennsylvania State University

SUMMARY

The emission of secondary electrons from dielectrics is subject to numerous effects of electric field which are experimentally difficult to control. Measurements have been reported using pulse techniques such that local fields do not build to significant levels, but measurements with fields present are also of interest. This paper describes a specific series of measurements under controlled conditions and examines their implications in terms of fields, magnitude and angle, near the dielectric surface. The measurements were made for a charged fluorinated-ethylene-propylene surface near a grounded aluminum half-round resting on the surface. The geometry produced a stable surface-charge gradient being controlled by a strongly enhanced secondary emission for which a model is constructed. Observations of surface flashovers under various conditions confirm the predictions of some scaling exercises.

INTRODUCTION

When a dielectric-metal interface is exposed to an electron beam, the dielectric surface becomes negatively charged (at least if the beam energy exceeds a few kilovolts) and potential gradients are established near the interface which is held at ground potential. Previous studies of the charge distribution and the associated potential contours are reported in reference 1 which describes the method of measuring the charge distribution and some typical results. Some distributions are more stable than others with stability expressed in term of the probability of flashover, a transient discharge where the accumulated charge is cleared from the dielectric surface. This paper examines the charge transfer processes near an interface so as to identify characteristics of a stable distribution of charge. The dielectric is a 0.127-mm (5-mil) sheet of fluorinated-ethylene-propylene with a metal backing.

The importance of secondary emission was emphasized in reference 1, yet at the time of that writing, pertinent data had not been attained. Summarized in figure 1 is a series of measurements (ref. 2) of secondary emission in the

*This work was supported by the National Aeronautics and Space Administration under grant NSG-3097.

presence of a normal field. These show that emission differs from the conventional, zero-field, characteristic (ref. 3). The field increases the critical potential (upper unity-crossing point) and thus reduces the steady state surface potential in a monoenergetic electron beam. This trend is consistent with the lowering which is observed near an interface but the observed lowering exceeds that attributable to normal electric fields. In the vicinity of the interface are found tangential as well as normal field components and, though the effect of tangential fields has not been measured, it is surmised that they account for the discrepancy.

A particular measured charge distribution is chosen as a reference data set and from this the equipotential lines and fields near the interface are calculated. Effects of perturbing or scaling this reference data set are examined and the critical potential for secondary emission is related to surface fields. From observations that microscopic structures trigger flashovers, one confirms the scaling predictions.

CALCULATING POTENTIAL PROFILES

From a measured distribution of potential on the surface of the dielectric, the equipotential curves and fields were calculated above the surface. The calculation depended of course on the nature of the interface which, for this discussion, is formed by placement of a half-round grounded aluminum strip on the surface of the dielectric sheet as shown in figure 2. As a first step in the calculation, the geometry was transformed by the conformal mapping $W = Z + 1/Z$ such that the surface became a plane. A Green's integral (ref. 4) was employed to generate values of potential and field above the plane and then the results were mapped back to the original geometry for display. This process, as described in reference 2, was implemented by representing the potential on the dielectric surface with an easily integrated piecewise-linear function. Because of this approximation, some irregularities in field data were observed, especially near the vertices of the piecewise-linear function. Also the influence of a ground plane placed several centimeters above the specimen was ignored. The calculational procedures were organized in two ways, one being to generate displays of equipotential contours and the other to tabulate surface fields at the midpoints between vertices. The latter output was used by an iterative program which sought to find a surface potential distribution that satisfied some criterion placed on the surface fields.

SURFACE MODELS

Charge does not reside precisely at the surface of the dielectric but rather in layers slightly below the surface. Katz et al (ref. 5) describe a buried electron layer and an electron depletion layer close to the surface. The electrons are buried, because of their impact energy, at several hundred angstroms yet secondaries escape from nearer the surface. Field patterns may be represented crudely by assuming discrete charge layers as shown in figure 3.

The weakest fields are those outside the dielectric yet they aid secondary emission as do the fields just below the surface. However should the external fields be reversed in direction, though weak they would stifle emission of secondaries. This is because secondaries are emitted with low kinetic energies, their range in dielectric being at most a few angstroms. Fields tangential to the surface will be the same on either side of the surface and they will often exceed the normal external field component. While realizing that the internal fields are perhaps 10 times as large we find that external normal fields 3 kV/mm significantly influence secondary emission. Because of the equality of tangential fields, the aiding sense of the internal normal field, and the dominance of the external field, the dielectric is modelled simply as a surface charge sheet.

Near interfaces, equipotential lines are nearly normal to the surface such that electrons are accelerated nearly parallel to the surface. An emitted secondary may, in traveling a few micrometers, gain enough energy to cause additional secondary emission. If it strikes the surface with a grazing angle it is an efficient producer of secondaries. When field lines are nearly parallel to the surface we thus find an efficient mechanism for electron emission. A quantitative description of how tangential fields affect secondary production is not available but nevertheless certain aspects of the phenomenum are indicated in the analyses which follow. The term, secondary emission, is used here to include the effects of avalanching so that a given primary may have a widespread effect on charge distribution. Regardless of the process, a steady state is gained when at all points charges emitted balance charges received.

STABLE CHARGE DISTRIBUTION

Shown in figure 4 is a piecewise linear representation of experimental data for a half-round radius of 1.2 mm. Experimental resolution was no better than 0.5 mm so that some liberty has been taken to form this representation. Data has been smoothed. When this data set is used in the routine which generates equipotential lines, results are as shown in figure 5. The figure is taken as a reference for later simulations and it represents a stable interface configuration. Several features are noteworthy. As surface potential approaches zero the equipotentials become more nearly normal to the surface such that secondary emission increases. More specifically we would say that the critical point shifts to higher voltages, approaching 20 kV at the interface. Furthermore the equipotentials become more closely spaced; tangential fields approach 50 kV/mm such that bulk conduction may be significant. If the inclination angle θ is defined as the angle between the surface and the equipotentials, then its variation with potential (fig. 6) summarizes the surface conditions.

SIMULATIONS

Although experimental data are crucial for explaining interface phenomena, they are obtained only with a substantial time investment and resolution is limited. The calculational routines permit a simulation of conditions not measured as well as hypothetical conditions not experimentally obtainable. Several important features have evolved from the simulations conducted.

One of the easiest exercises was to assume the same surface potential distribution in the presence of smaller half-rounds. Results for a 0.24-mm radius are compared with the reference condition in figure 6. With the same distribution and a smaller half-round the angles are greater and the distribution of charge is not expected to be in steady state. Rather the charge distribution will shift toward a new equilibrium in a manner to be determined.

Whereas figure 6 was drawn for a given surface potential near different sizes of half-round, it may just as well represent scaled surface potentials near half-rounds of the same size. When such an interpretation is used we conclude that a steeper gradient corresponds to lesser angles. If now we reconsider our reference distribution near a half-round of reduced size, we expect the potential gradient to increase and the angles to relax toward the reference case.

Assuming that, when the half-round is made smaller, the charge distribution becomes steeper, we may anticipate a high-field limit where stable conditions no longer exist. This may also be argued another way. The equipotential lines of figure 5 may be scaled along with the half-round and no changes in potential or angle will be perceived though electric fields will change inversely with dimensions. Expermentally we have tested two configurations that by this scaling procedure would produce fields much higher than the reference case. For one of the tests, a .25-mm (10-mil) wire was laid across the surface of an otherwise stable system. For the other a slit was cut in the dielectric and conductive epoxy was forced from the underside through the slit to form a bead somewhat resembling a half-round. We have found that neither configuration allows formation of a stable charge. Flashovers occur at relatively low voltages during the charging process and full charge at 20 kV is never reached. It is significant to note that when epoxy was applied and hardened before the slit was cut, the distribution near the slit was stable.

One might argue that if secondary emission is a highly sensitive function of θ near $\theta = 90°$ then for a stable configuration θ will be within perhaps a few degrees of 90 for most of the range of potentials. On this basis one could let θ be 90° as a first approximation and calculate what the charge distribution must be for this condition to hold. Possibly figure 6 is very sensitive to experimental errors and should be discounted. This possibility was tested by programming an iterative routine which shifted the data points of figure 4 until all points (but one) of figure 6 were within 4 degrees of 90. The potential distribution attained in this way is compared with the reference distribution in figure 4. The discrepancy between the

curves is several times what can be attributed to experimental errors and thus the assumption $\theta = 90°$ is not a good one. Another trial requiring that $\theta = 80°$ led to similar results. The angle θ is not constant but decreases as surface potential increases.

Equipotential curves are shown in figure 7 for the assumed condition that fields will be tangential to the surface. The somewhat plausible argument in support of tangential fields is rebuffed by comparison with the experimental data represented in figure 5. In figure 7, the curve for -1 kV is not normal as are the others. Though an attempt was made to force conformity, the iterative computation became unstable and the effort was abandoned.

PHYSICAL IMPLICATIONS

From the preceding material, a model of the secondary emission characteristics emerges. Assumptions are made that the steady state potential corresponds to the condition of a unity secondary emission coefficient, that the secondary critical voltage is a unique function of field strength and angle, and equivalently that secondary avalanches are relatively insignificant. All illustrations are based on 20-kV electron fluxes so that, in a steady state, surface voltage V_s and critical voltage V_c are related by $V_c - V_s = 20$. In a transient situation the equality is violated yet it is assumed nevertheless that

$$V_c = f(E, \theta)$$

where the function of field strength E and θ is still considered to exist. If $20 + V_s$ is less than V_c, electrons will arrive with some energy less than the critical value and the surface will lose charge until a steady state is attained. If $20 + V_s$ is higher, charge will accumulate. From an assumed perturbation in a potential distribution changes in E and θ can be found. For stability the corresponding change in V_c must be of the proper polarity and thus constraints are placed on f.

Perturbations are represented as lateral displacements of the reference data points shown in figure 4. Each point is thus identified with a given V_s and a variable coordinate. The perturbation illustrated here consists of expanding the reference distribution by 25 percent while holding the half-round constant. Using changes in E and θ we may calculate ΔV_c in terms of the partial derivatives f_E and f_θ:

$$\Delta V_c = f_E \Delta E + f_\theta \Delta\theta$$

For restoration of the reference distribution, charge must accumulate on the surface and consequently the following condition must be met:

$$V_c - V_s < 20 \text{ or } \Delta V_c < 0$$

Anticipating that both f_E and f_θ are positive, we require that $f_E \Delta E$ be the dominant term.

A possible function $f(E,\theta)$ is shown in figure 8 along with the reference data from figure 6. It is drawn so that the partial derivatives are positive and so that it conforms to the reference distribution. It is notable that the slope of the constant-E lines must be less than the slope of the reference curve if f_E is to be positive. Otherwise the slope is not clearly specified. The function is shown to decrease as θ increases beyond 90° because the normal field component opposes secondary emission. Focusing our attention on the point at $V_s = -7$, we may estimate partial derivatives to be

$$f_\theta = 0.06 \text{ kV}$$

$$f_E = 0.14 \text{ mm}$$

At this point the perturbation produces changes of $\Delta E = -3.37$ kV/mm and $\Delta\theta = 1.19°$. The change ΔV_c then has the value -0.4 kV which is of the desired polarity. For the function illustrated in figure 8, the values of ΔV_c are all negative and the assumed perturbation should relax toward the reference condition. Details are shown in Table I. This function cannot be used as a quantitative representative of secondary emission characteristics because it is not sufficiently supported by data. Rather it is a qualitative model which suggests how a greater data base might be used in developing an accurate description.

When θ is near 90°, the occurrence of avalanches may disallow the use of $f(E,\theta)$ as a representative of critical voltage. The size (< 0.1 mm) of this region precludes using the experimental procedures of reference 1 to attain more detailed information. Consequently any use of the model near 90° is highly speculative. However for lesser angles, secondary electrons have little probability of returning to the dielectric surface and the concept of critical voltage is justifiable. Further experimentation should provide a detailed description of $f(E,\theta)$.

EXPERIMENTAL DETAILS

In all cases where flashover probability was high, the cause of flashover could be ascribed to some fine detail in the interface. When care was taken to avoid or remove the causative feature, then surface charge distributions stablized. Several examples are described in this section.

A stable distribution was attained by covering the dielectric sheet with a metal aperture plate having a thickness of 1 to 1.5 mm. Occasional flashovers were accompanied by light flashes on the edge of the hole cut in the plate. As time passed, flashovers became less frequent because, it is presumed, the rough spots on the edge were eroded. After extensive exposure

to beams of high flux, the dielectric surfaces were found to be coated near the interface with a nonconductive-whitish substance thought to be aluminum oxide. Figure 9 is a microphotograph illustrating the deposit.

When an aperture plate was cut in half and assembled by butting edges, flashover probability was high unless care was taken to align the joints properly. When assembly was sloppy, light flashes at the joint accompanied the flashovers.

Half-rounds were inserted and clamped between the halves of split aperture plates. The charge distributions were stable except for possible joint effects. However when a fine wire was used instead of a half-round, the wire became the cause of flashovers.

Several specimens were prepared with slits or punctures which exposed the underlying ground plane through the dielectric sheet. When the underlying conductive coating was bonded with conductive epoxy to a rigid metal substrate, the cutting of slits or holes did not, at first, cause flashover rates to become high. Yet as these specimens aged, flashovers became more frequent. Light flashes concentrated on specific spots along the slits, the repetitive discharges eroded dielectric, and the spots became trigger points for discharges. One such spot formed at the end of a slit as illustrated in figure 10.

When a slit was cut before the epoxy and backing plate were applied, the epoxy oozed through the slit and formed a bead on the exposed surface of the epoxy. This configuration was unstable from the beginning.

CONCLUDING REMARKS

Measured surface potentials near dielectric-metal interfaces provide a basis for the modelling of secondary emission phenomena reported here. Measurements of secondary emission from the dielectric show that normal electric fields increase the critical voltage, that point where the emission coefficient is unity. Assuming that, for steady state, the coefficient is unity under all field conditions we then calculated the critical voltages at the various values of field magnitude and angle represented by the measured distribution. A model, based on this limited data, shows that critical voltage increases with both the field magnitude and the angle between the surface and equipotential lines. Scaling exercises predict increasing field strengths as the size of a ground strip is reduced. Corresponding experiments show that surface charge distributions become less stable.

REFERENCES

1. Robinson, J. W.: Charge Distributions Near Metal-Dielectric Interfaces Before and After Dielectric Surface Flashover. Proceedings of the Spacecraft Charging Technology Conference, pp. 503-515, 24 February 1977.

2. Quoc-Nguyen, N.: Secondary Electron Emission from a Dielectric Film Subjected to an Electric Field. NASA CR-155231, Nov. 1977.

3. Willis, R. F. and Skinner, D. K.: Secondary Electron Emission Yield Behavior of Polymers. Solid State Communications 13, pp. 685-688, 1973.

4. Jackson, J. D.: Classical Electrodynamics, 2nd ed. Wiley, pp. 40-44, 1975.

5. Katz, D. E. et al.: A Three Dimensional Dynamic Study of Electrostatic Charging in Materials, NASA CR-135256, August 1977.

TABLE I - THE CHANGE ΔV_c CORRESPONDING TO AN ASSUMED PERTURBATION

Potential	Reference		Change		f_E	f_θ	ΔV_c
	E	θ	ΔE	Δθ			
kV	kV/mm	degrees	kV/mm	degrees	mm	kV	kV
- 1	48.17	105.44	-9.67	0.26	--	--	--
- 3	32.73	81.13	-6.63	0.55	0.11	0.06	-0.70
- 5	26.71	64.47	-5.50	0.76	0.11	0.06	-0.56
- 7	15.69	50.44	-3.37	1.19	0.14	0.06	-0.40
- 9	9.01	45.25	-2.06	1.91	0.3	0.06	-0.50
-11	5.68	45.55	-1.35	2.73	0.6	0.06	-0.65

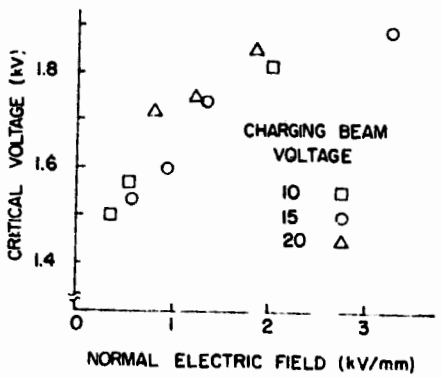

Figure 1. - Secondary emission critical voltage as function of normal field outside surface.

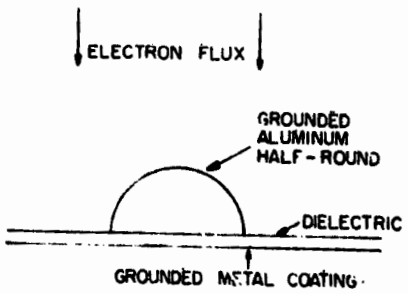

Figure 2. - Configuration used for experiment and simulation.

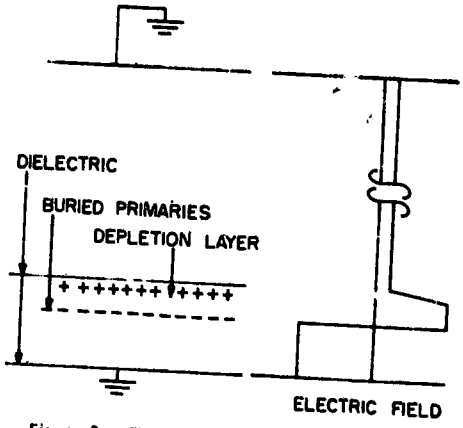

Figure 3. - Field configuration near dielectric surface.

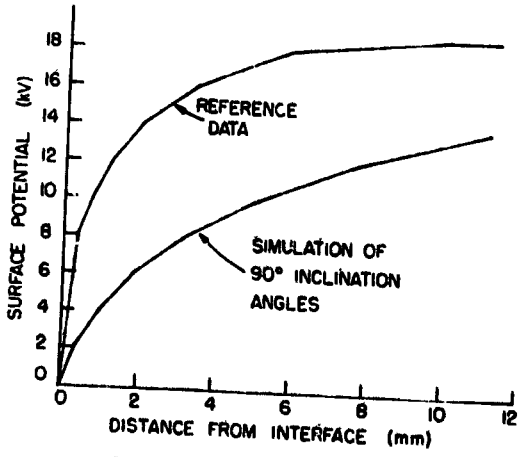

Figure 4. - Dielectric surface potential.

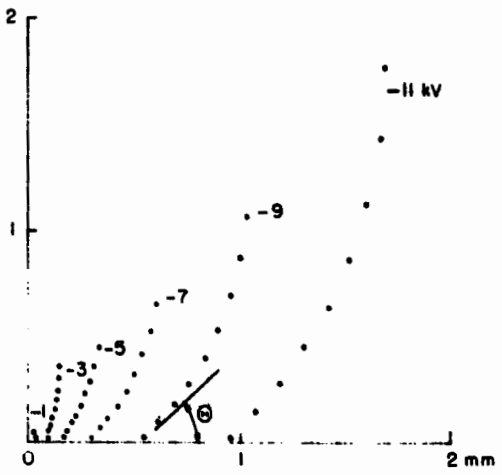

Figure 5. - Equipotential contours for reference distribution near half-round.

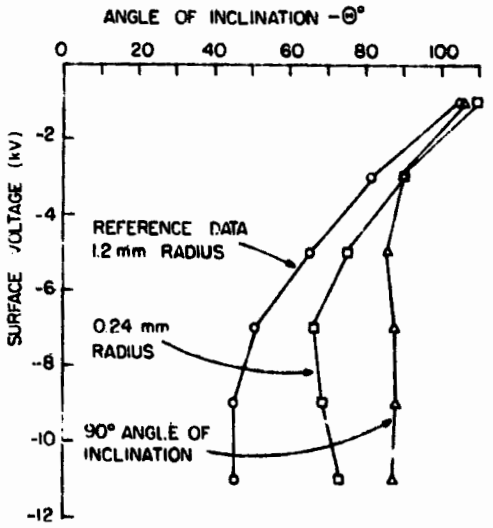

Figure 6. - Summary of surface conditions.

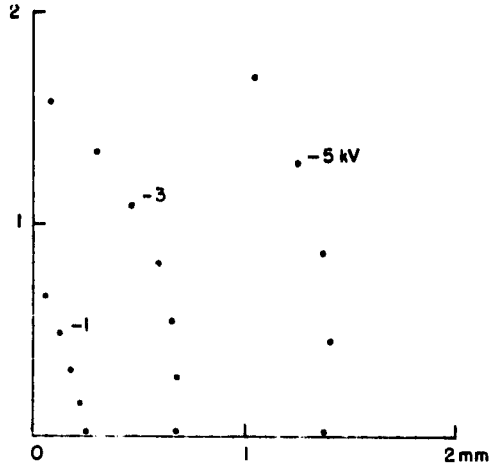

Figure 7. - Equipotential contours with 90° angles of inclination.

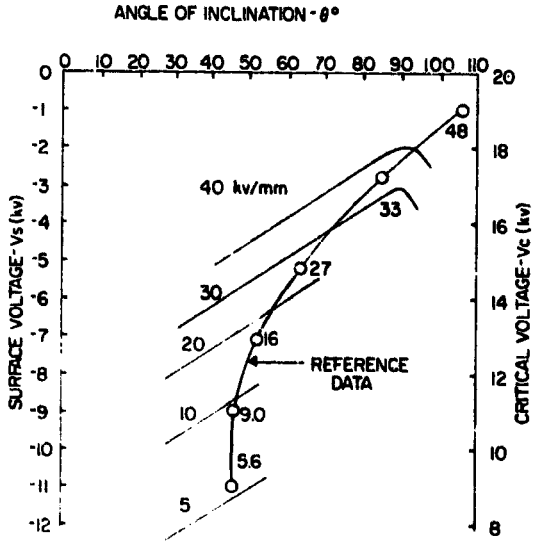

Figure 8. - Critical voltage function conforming with reference data.

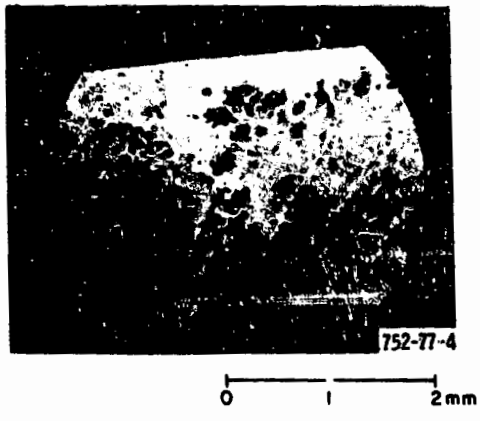

Figure 9. - Coating near edge of aperture plate.

Figure 10. - Erosion pit at end of slit.